Interaction of Ozone and Water Vapor with Spark Discharge Soot Aerosol Particles Coated with Benzo[*a*]pyrene: O_3 and H_2O Adsorption, Benzo[*a*]pyrene Degradation, and Atmospheric Implications

Ulrich Pöschl,* Thomas Letzel, Christian Schauer, and Reinhard Niessner

Technical University of Munich, Institute of Hydrochemistry, Marchioninistrasse 17, D-81377 Munich, Germany

Received: November 9, 2000; In Final Form: January 31, 2001

The interaction of ozone and water vapor with spark discharge soot particles coated with the five-ring polycyclic aromatic hydrocarbon benzo[*a*]pyrene (BaP) has been investigated in aerosol flow tube experiments at ambient temperature and pressure (296 K, 1 atm). The investigated range of ozone volume mixing ratio (VMR) and relative humidity (RH) was 0−1 ppm and 0−25%, respectively. The observed gas-phase ozone losses and pseudo-first-order BaP decay rate coefficients exhibited Langmuir-type dependencies on gas-phase ozone concentration and were reduced in the presence of water vapor, which indicates rapid, reversible and competitive adsorption of O_3 and H_2O on the particles followed by a slower surface reaction between adsorbed O_3 and BaP. At low ozone VMR and RH, the half-life of surface BaP molecules was found to be shorter than previously reported (∼ 5 min at 30 ppb O_3 under dry conditions). At higher RH and for multilayer BaP surface coverage, however, a strong increase of BaP half-life was observed and can be attributed to competitive H_2O adsorption and to surface/bulk shielding effects, respectively. From four independent sets of ozone loss and BaP decay measurement data the following parameters have been derived: O_3 and H_2O Langmuir adsorption equilibrium constants $K_{O_3} = (2.8 \pm 0.2) \times 10^{-13}$ cm^3 and $K_{H_2O} = (2.1 \pm 0.4) \times 10^{-17}$ cm^3, maximum pseudo-first-order BaP decay rate coefficient $k_{1,4} = (0.015 \pm 0.001)$ s^{-1}, adsorption site surface concentration $[SS]_S = (5.7 \pm 1.7) \times 10^{14}$ cm^{-2}. On the basis of these values, a second-order BaP−O_3 surface reaction rate coefficient $k_{2,s} = (2.6 \pm 0.8) \times 10^{-17}$ cm^2 s^{-1} can be calculated, and estimates for the mean surface residence times and adsorption enthalpies of O_3 and H_2O have been derived: $\tau_{O_3} \approx 5-18$ s; $\tau_{H_2O} \approx 3$ ms, $\Delta H_{ads,O_3} \approx -(80-90)$ kJ mol^{-1}, $\Delta H_{ads,H_2O} \approx -50$ kJ mol^{-1}. The results and their atmospheric implications are discussed in view of related studies.

Introduction

Polycyclic aromatic hydrocarbons (PAH) are ubiquitous in the atmosphere as well as in other environmental compartments. They originate mostly from incomplete combustion of fossil fuels and biomass, and PAH consisting of more than four fused aromatic rings reside to a large extent on fine combustion aerosol particles.[1] Since these particles can be deposited in human lungs[2] and since several PAH and some of their degradation products are known to have a high carcinogenic, mutagenic, and allergenic potential, they are of major interest with respect to air pollution control.[1,3] Benzo[*a*]pyrene (BaP), a PAH with the chemical formula $C_{20}H_{12}$ consisting of five six-membered aromatic rings, is one of the most powerful carcinogens among the 16 U.S. Environmental Protection Agency (EPA) "Priority Polycyclic Aromatic Hydrocarbon Pollutants" and occurs in chimney soot as well as in atmospheric particulate matter. The atmospheric fate of particle-associated PAH has been investigated in numerous studies, and due to its high toxicological relevance BaP is among the most intensively studied compounds of this class. However, the chemical mechanism and kinetics of BaP degradation by ozone are still poorly understood, and a wide range of partly conflicting experimental results and interpretations have been reported,[1,4] as will be detailed in the discussion section.

Besides their relevance as toxic air pollutants, polycyclic aromatic compounds (PAC = PAH + derivatives) at the surface of combustion aerosol particles can influence these particles' interaction with reactive trace gases and water vapor, their activity as condensation nuclei, their atmospheric residence times, and consequently their direct and indirect climatic effects.[5−7] Moreover PAC represent well defined soot model substances, since the basic structure of soot can be regarded as an agglomerate of graphene layers which are effectively the same as high molecular mass PAC.[8]

The atmospheric importance of soot and other types of black carbon has been discussed in numerous recent publications. Black carbon accounts for most of the light absorption by atmospheric aerosols and influences their climatic effects. Besides direct radiative effects local heating of air masses induced by soot aerosol pollution may also lead to a reduction of cloudiness.[9−11] On the other hand atmospherically aged soot particles may act as cloud condensation nuclei and thus lead to radiative cooling effects, even though freshly emitted soot particles are known to be rather hydrophobic.[12,13]

Soot aerosols also have been pointed out as a potentially important sink for atmospheric ozone. Recent studies, however, indicate that the effect of soot on the atmospheric ozone concentration may be insignificant.[14−16] Nevertheless, chemical processing by ozone and other photooxidants can strongly affect the surface properties and interaction of soot and other carbon-

* Corresponding author. E-mail: ulrich.poeschl@ch.tum.de. WWW: http://www.ch.tum.de/wasser/aerosol. Tel/Fax: +49−89−7095−7996/7999.

10.1021/jp004137n CCC: $20.00
Published on Web 03/31/2001

aceous aerosol particles with water vapor[12,13] and thus influence their average atmospheric residence times which are estimated to be on the order of 1 week.[17] Moreover heterogeneous reactions on soot particles were found to produce HONO,[18,19] and PAC, in particular phenols, at the soot surface are thought to be of primary importance for these reactions.[20]

The actual effect of soot on the radiative and chemical budgets of the atmosphere is still poorly known. Some of this uncertainty is due to a lack of knowledge about the physicochemical properties of soot, and one of the major problems is the fact that soot is not a well-defined chemical substance. Technically it is defined as the black solid product of incomplete combustion or thermal decomposition of hydrocarbons, and depending on the source (combustion conditions or fuel composition) and on aging processes the structure and composition of soot aerosol particles can vary considerably.[21]

The chemical composition of the fine carbon aerosol particles, which were produced by a spark discharge generator and used as model soot carriers for benzo[*a*]pyrene in this work, is hardly the same as the composition of typical diesel soot particles in the atmosphere. Nevertheless the predominant chemical structure of the spark discharge soot particles (aromatic carbon rings arranged in graphene- or PAC-like layers), which can be generated with excellent reproducibility, can be regarded as a reasonable proxy for the refractory core of real soot particles.[15]

The interaction of ozone with different model soot substances has been investigated in several previous studies, which will be discussed below. In some of these studies spark discharge soot has already been used and was found to have similar properties as the other model soot substances like charcoal, channel black, or *n*-hexane soot.[15,22]

In the present study the interaction of O_3 and H_2O with spark discharge soot particles coated with benzo[*a*]pyrene and the resulting BaP decay and ozone loss have been investigated for the first time in an aerosol flow tube experiment under well-defined conditions. A detailed mechanistic interpretation of the experimental results is given and discussed in view of related previous studies.

Experimental Section

Aerosol Generation and Reaction System. The model soot aerosol was produced by a spark discharge generator (GfG 1000, Palas)[23] with graphite electrodes (diameter 6.15 mm, 99.9995% C, Johnson Matthey). The generator was operated with argon carrier gas (99.996% Ar, Messer-Griesheim) at a volumetric flow rate of 6.5 L min^{-1} and at a discharge frequency of 100 Hz. As shown in Figure 1 the aerosol was fed into a buffer reservoir (5 L three-neck flask), and a flow of 2.0 L min^{-1} was passed through an aerosol neutralizer (^{85}Kr, model 3077, TSI) into a benzo[*a*]pyrene particle coating unit based on the condensation technique described by Niessner.[24] To adjust the particle number concentration in the reaction system, a variable fraction of this flow was passed through a particle filter before entering the coating unit, which consisted of a temperature controlled BaP-reservoir and a ring gap mixing nozzle followed by a condenser cooled to 279 K. In the ring gap mixing nozzle the argon aerosol carrier flow was mixed with a nitrogen flow (2.0 L min^{-1}, 99.9990% N_2, Air Liquide) carrying benzo[*a*]-pyrene vapor from the BaP reservoir into the condenser.

After the particle coating unit a fraction of 2.6 L min^{-1} of the aerosol flow was mixed with another nitrogen flow saturated with water vapor (0 or 1.3 L min^{-1}, relative humidity >95%) and with an oxygen/ozone flow (1.3 or 2.6 L min^{-1}, 99.95% O_2, O_3 volume mixing ratio 0−4 ppmv). Then the reaction mixture was introduced into an aerosol flow tube (i.d. 11 cm, length 120 cm with conic entrance and exit junctions of 35 cm each) operated under laminar flow conditions at ambient pressure and temperature (1 atm, 296 K, Reynolds number ∼70). The residence time in the flow tube was controlled by a movable sampling orifice, which could be set to different axial positions at 0 to 100 cm distance from the flow tube entrance and consisted of a glass cone (o.d. 10 cm) mounted on a Teflon sled. The sampling flow (volumetric flow rate 4.5 L min^{-1}) was passed through two consecutive scrubber-type diffusion denuders filled with activated carbon (p.a., grain size 4−8 mm, Fluka) to remove excess ozone, and finally the particles were sampled on glass fiber filters (GF/C 47 mm, Whatman) mounted in a stainless steel filter holder (self-made). At the downstream end of the flow tube the excess flow was vented into a laboratory hood.

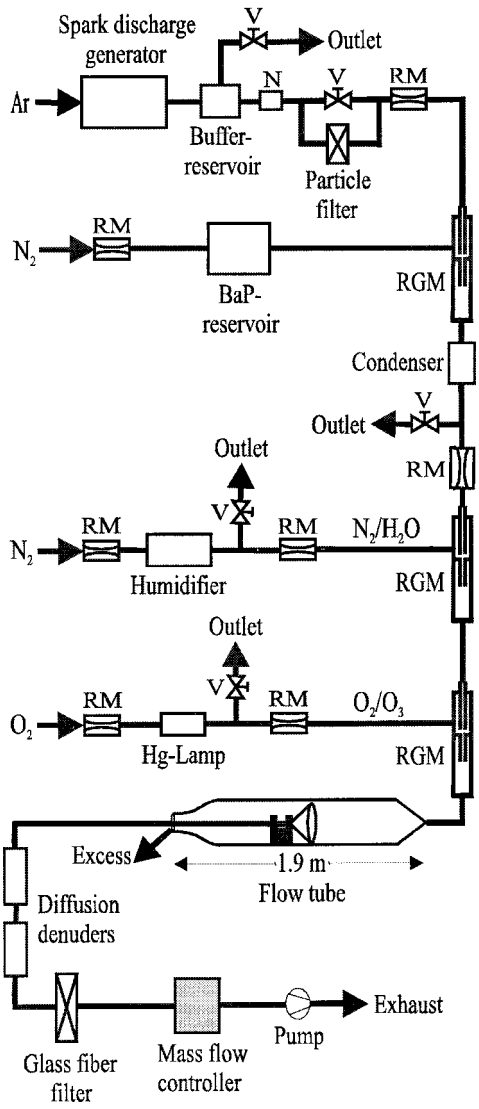

Figure 1. Experimental setup: aerosol generation, flow tube reactor and sampling system (RM: rotameter; V: valve; N: aerosol neutralizer; RGM: ring gap mixing nozzle).

Ozone was generated by UV irradiation of the oxygen flow with a mercury vapor lamp.[25] The ozone volume mixing ratio (VMR) was controlled by varying the oxygen flow and the intensity of UV irradiation with an adjustable aperture. For the measurements under humid conditions, the water vapor carrier gas flow was saturated by passing through a washing bottle filled with deionized water, and a relative humidity (RH) of (25 ± 3)%

was established in the aerosol flow tube. For the measurements under dry conditions the water vapor carrier flow was turned off, and the relative humidity in the reaction system was <1%.

Flow tube, sampling cone, mixing nozzles, condenser, aerosol buffer, BaP, and water reservoirs were made of Pyrex glass. The diffusion denuders consisted of a Pyrex glass jacket with a central tube of fine steel mesh. Antistatic Tygon tubing (Norton) was used for all aerosol flow connections between the glass components, and Teflon tubing was used for the ozone carrier flow. The sampling gas flow was controlled by a mass flow controller (VVS 0/22, Gossen), all other flows were monitored by rotameters (Rota-Yokogawa) and adjusted with tube clips. A commercial photometric ozone analyzer (O_3 41 M, Ansyco), a capacitive humidity sensor (FH A646−1, Ahlborn), and a condensation particle counter (model 3020, TSI) were used to monitor the gas and particle number concentrations throughout the reaction system.

From the entrance of the aerosol flow tube to the sampling orifice all concentrations except for BaP were practically constant, i.e., under the experimental standard conditions described in the results section no significant changes of ozone, water vapor, and particle number concentration were observed between the different sampling positions along the flow tube (0−100 cm, variations < 5%). In the scrubber-type diffusion denuders, i.e., between the sampling orifice and the filter holder, particle number and water vapor concentration were reduced by a constant fraction of 10%, and the ozone concentration was reduced by ≥95%.

The mean residence time of the aerosol particles in the flow tube and in the other elements of the reaction system was determined experimentally from the 60% value of the sigmoid particle concentration increase after connection of the particle flow, which is typical for nonideal flow tube reactors.[26] The slope of the linear increase with sampling position was 0.66 s/cm with a standard error of 10%. The mean residence times in the tube connections, diffusion denuders and in the filter holder were weighted by the average ratio of the ozone VMR in the respective element relative to the VMR in the flow tube (first denuder 0.65, second denuder 0.20, filter holder 0.04) and summed up to obtain the effective reaction time at sampling position zero. This was 26 s in the presence of ozone, while for the zero-ozone data points measured at the beginning and at the end of every kinetic measurement run as described below the effective reaction time was set to zero. During the experiments aerosol generation and reaction system were generally kept in the dark, and also the aerosol sampling and analysis described below was performed without irradiation by strong light sources.

Aerosol Sampling and Analytical Methods. Prior to use the glass fiber filters were heated to 500 °C for 2 h in a muffle furnace to remove organic contaminants. In the BaP degradation kinetic experiments the aerosol particle number concentration in the flow tube was generally kept at $(1.5 \pm 0.3) \times 10^5$ cm^{-3} and three aerosol filter samples were collected at every sampling position, each of them with a sampling volume of 22.5 L (5 min at 4.5 L min^{-1}) which corresponds to a total number of $\sim 3 \times 10^9$ particles. After particle collection the filter samples were transferred into brown glass screw-cap vials (4 mL, NeoLab) and spiked with 11.8 ng of triphenylene (Ehrenstorfer) dissolved in 10 μL of methanol (LiChrosolv, Merck), which served as an internal standard. The filters were extracted with 3 mL of a toluene-dichloromethane-methanol solvent mixture (1:1:1 v/v/v; LiChrosolv, Merck) for 15 min in an ultrasonic bath. Then the filters were removed and the solution was evaporated to ~0.5 mL under a nitrogen gas flow. To remove particulates, the remaining solution was passed through Pasteur pipets filled with filtration glass wool (Roth) and collected in tapered HPLC vials (Chromacol 1.1 mL, Supelco). Under nitrogen the solution was evaporated to dryness, and the residue was dissolved in 200 μL of methanol and analyzed by high performance liquid chromatography (HPLC) with fluorescence detection. The HPLC system from Shimadzu (two pumps LC-6A, controller SCL-6B, auto-injector SIL-6B, column oven CTO-10A, fluorescence detector RF 551) was equipped with a reversed phase chromatographic column (Envirosep PP 125 × 4.6 mm, Phenomenex). The injection volume was 20 μL, the column oven temperature was 293 K, and the elution was isocratic with an acetonitrile−water mixture (85:15 v/v; LiChrosolv, Merck) at a constant flow rate of 2 mL min^{-1}. The retention times for the internal standard triphenylene and for benzo[*a*]pyrene were 3 and 12 min, and the fluorescence excitation/detection wavelength pairs were 258 nm/354 nm and 297 nm/403 nm, respectively. The integration of the chromatographic peak areas was performed with the software package CLASS−VP (Shimadzu). For the quantification of triphenylene and BaP the HPLC system was calibrated with a series of standard solutions, and straight calibration lines of peak area vs concentration were obtained in the range from a few pg μL^{-1} up to a few ng μL^{-1}. The detection limits were 3 pg μL^{-1} for BaP and 6 pg μL^{-1} for triphenylene. Assuming equal relative losses of triphenylene and BaP during the clean up process, the triphenylene recovery, which was generally on the order of 70%, was used to correct the BaP peak area to 100% recovery. The total amount of BaP in the analyzed filter sample was then calculated based on the corrected peak area, the calibration line, and the HPLC sample volume. Carbon content measurements of aerosol filter samples were performed according to the VDI standard procedure[27] by thermochemical analysis with coulometric CO_2 detection (Coulomat 702, Ströhlein). Aerosol particle size distributions were measured with a differential mobility analyzer (DMPS, model 3932, TSI), consisting of an electrostatic classifier (model 3071, TSI) combined with an ultrafine condensation particle counter (model 3025, TSI) and a personal computer for data collection and analysis.

Results

Aerosol Particle Characterization and Benzo[*a*]pyrene Surface Coverage. The standard conditions maintained during all experiments described below unless explicitly mentioned otherwise were as follows: BaP reservoir temperature $T_{BaP} = (353 \pm 0.2)$ K, flow tube temperature (296 ± 2) K, particle number concentration in the flow tube $(1.5 \pm 0.3) \times 10^5$ cm^{-3}. The model soot aerosol exhibited a log-normal particle size distribution with mobility equivalent count median diameters σ_g of 86 nm at the flow tube entrance and 90 nm at the filter holder, respectively. In both cases the geometric standard deviation σ_g was 1.7, and the values were the same under dry and humid conditions. The apparent particle size increase of 4 nm is within the DMPS measurement uncertainty of about ± 5% and thus in agreement with the < 3% increase expected from coagulation.[28]

To determine the average particle mass m_p, which is defined as the proportionality factor between particle number and mass concentration, the carbon content of filter samples of the model soot aerosol was measured according to the VDI standard procedure for thermal analysis of total carbon (TC) and elemental carbon (EC).[27] Four samples were collected, each of

them with a sampling volume of 540 L (2 h at 4.5 L min^{-1}). The mean particle number concentration in the sampling flow was 1.1×10^6 cm^{-3} and the average TC mass deposited on the filters was 100 μg with a standard deviation of 4 μg and an EC fraction of 70−80%. Assuming that the particle mass was dominated by TC and that the number of particles collected on the filter equals the average number concentration in the sampling flow times the sampling volume, an estimate of 1.6×10^{-16} g was calculated for m_p. Because of the above assumptions this value represents a lower limit. On the other hand enhanced coagulation should increase m_p at a particle number concentration of 1.1×10^6 cm^{-3} by about 10% relative to the experimental standard conditions.[28] However, in view of the overall uncertainty of m_p, which is dominated by the uncertainty of the total number of collected particles and estimated to be on the order of ± 15%, the coagulation effect is neglected and $m_p = 1.6 \times 10^{-16}$ g will be used below.

Estimates for the average particle surface area of the model soot aerosol S_P, which is defined as the proportionality factor between particle number and surface area concentration, were obtained by two different approaches. In the first approach the average particle mass was multiplied with the literature value for the specific surface of the spark discharge soot produced by the generator type used in this study (395 m^2 g^{-1}),[23] which led to an average particle surface area of 6.3×10^{-10} cm^2. In the second approach, diameters of average area d_a were calculated from the mobility equivalent count median diameters and geometric standard deviations of the measured log-normal particle size distributions ($d_a = d_g \exp(\ln^2\sigma_g)$).[29] With $d_a = 119$ nm, respectively, an average surface area of 4.5×10^{-10} cm^2 was obtained assuming spherical geometry of the aerosol particles ($S_P = d_a^2\,\pi$). Since the model soot particles produced by the spark discharge generator are known to have a fractal geometry consisting of primary particles with diameters on the order of 5 nm,[23] the average surface area calculated under the assumption of spherical geometry has to be considered as a lower limit. Thus, $S_p = 6.3 \times 10^{-10}$ cm^2 was used for all further calculations unless mentioned otherwise. The potential systematic error of this value is estimated to be less than ± 30%, since according to Kamm et al.[15] the used specific surface literature value of 395 m^2 g^{-1} can be regarded as an upper limit, while the estimated error of the average particle mass is on the order of ± 15% and the lower limit derived from the mobility equivalent diameter is lower by about 30%.

To calculate the BaP surface concentration of the model soot aerosol particles, $[BaP]_S$, the total amount of BaP was divided by the total number of particles deposited on the investigated filter sample and by the average particle surface area. Under the experimental standard conditions ($T_{BaP} = 353$ K) and with $S_p = 6.3 \times 10^{-10}$ cm^2 the initial BaP surface concentration $[BaP]_{S,0}$ was $(1.8 \pm 0.3) \times 10^{13}$ cm^{-2}. These values represent the average and the standard deviation of forty zero-ozone data points measured at the beginning and at the end of the kinetic measurement runs described below. For five other BaP reservoir temperatures ranging from 327 to 373 K, $[BaP]_{S,0}$ was calculated as the average of two zero-ozone data points which agreed within ≤ 20% as indicated by the error bars in Figure 2. The different temperatures and mean values of $[BaP]_{S,0}$ are shown in Table 1. No BaP was detected in samples of uncoated spark discharge soot.

Assuming an even distribution of the BaP surface molecules with a molecular cross section of $\sigma_{BaP} = 1$ nm^2,[30] a BaP surface monolayer corresponds to $[BaP]_S = 1 \times 10^{14}$ cm^{-2}. Thus, $[BaP]_{S,0}$ was divided by this value to obtain the initial BaP surface coverage in units of monolayers $\theta_{BaP,0}$ as listed in Table 1. For the experimental standard conditions an initial surface coverage of about 0.2 monolayers was calculated with $S_p = 6.3 \times 10^{-10}$ cm^2, and even with the lower particle surface estimate $\theta_{BaP,0}$ would have been only 0.3. In contrast, a double monolayer coverage was calculated for $T_{BaP} = 373$ K. In Figure 2 $[BaP]_{S,0}$ is plotted on a logarithmic scale versus $1/T_{BaP}$. On the basis of the Clausius−Clapeyron equation and assuming that the carrier flow passing through the BaP reservoir is saturated with BaP vapor, the sublimation enthalpy of BaP can be calculated from the slope of the displayed linear least-squares fit. The calculated value of (118 ± 5) kJ mol^{-1} is in excellent agreement with the extrapolated literature value of (118 ± 2) kJ mol^{-1}.[31]

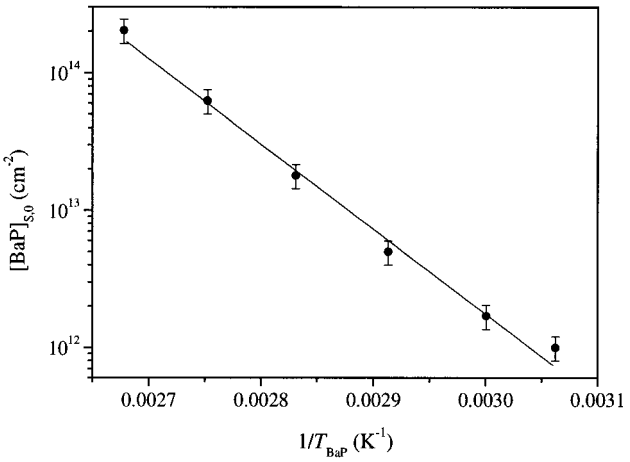

Figure 2. Initial BaP surface concentration on the spark discharge soot aerosol particles as a function of inverse BaP reservoir temperature. The error bars are ± 20%, representing the maximum observed deviations. The straight line is an exponential least-squares fit based on the Clausius−Clapeyron equation.

TABLE 1: BaP Reservoir Temperatures, Surface Concentrations, and Fractional Surface Coverages on the Spark Discharge Soot Aerosol Particles

T_{BaP} (K)	$[BaP]_{S,0}$ (10^{13} cm^{-2})	$\theta_{BaP,0}$
327	0.01	0.01
333	0.17	0.02
343	0.50	0.05
353	1.8	0.2
363	6.3	0.6
373	20	2

Benzo[*a*]pyrene Degradation Kinetics. Twenty kinetic measurement runs were performed to characterize the BaP decay at different ozone and water vapor concentrations under the experimental standard conditions defined above. During all of these runs the initial BaP surface coverage was on the order of 0.2 monolayers, while the ozone volume mixing ratio (VMR) in the flow tube was varied from 0 to 1 ppm and the relative humidity (RH) was kept either below 1% or at (25 ± 3)%. Even at the lowest nonzero ozone VMR of 27 ppb, the gas-phase ozone concentration, $[O_3] = 6.7 \times 10^{11}$ cm^{-3}, was still more than 2 orders of magnitude higher than the initial BaP concentration, $[BaP]_0 = 1.5 \times 10^9$ cm^{-3}. Thus, the ozone concentration can be regarded as a constant and included into an apparent BaP decay rate coefficient (isolation method). The constancy of $[O_3]$, i.e., its independence of sampling position and reaction time, was confirmed by the test measurements described in the Experimental Section.

Every kinetic measurement run consisted of five to nine data points, and each data point represents three filter samples

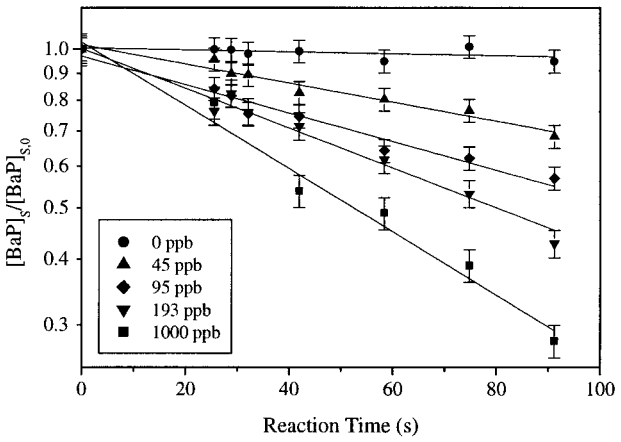

Figure 3. Representative BaP decays observed at different ozone volume mixing ratios under dry conditions. Normalized BaP surface concentrations are plotted against reaction time. The data points and error bars represent the means and standard deviations (± 1 s.d.) of the triplicate sampling and analysis performed at every sampling position. The straight lines are exponential least-squares fits based on pseudo-first-order rate equations.

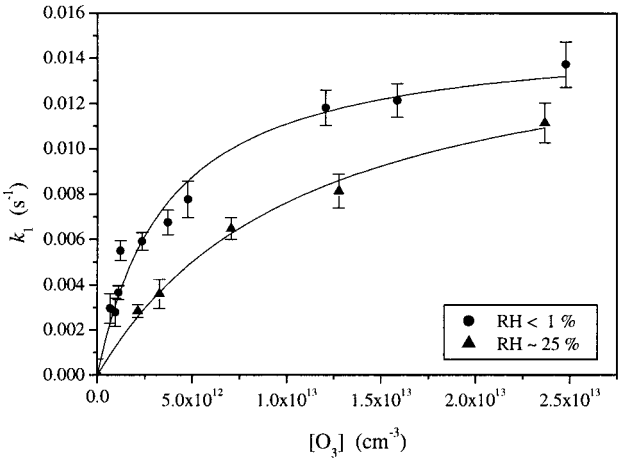

Figure 4. Pseudo-first-order BaP decay rate coefficients as a function of gas-phase ozone concentration. The upper data set was measured under dry conditions, the lower one at 25% relative humidity. The error bars represent the standard error of the slope of the corresponding BaP decay plots (± 1 s.e.). The curves are nonlinear least-squares fits based on Langmuir adsorption isotherms (eqs 9 and 15).

collected at a given sampling position. At the beginning an initial zero-ozone data point was measured at the 0 cm sampling position with the lamp of the ozone generator turned off. Then the lamp was turned on, the ozone VMR was adjusted and filter samples were collected at different sampling positions, usually with the sequence 0 cm−50 cm−100 cm−75 cm−25 cm. At the end the lamp was turned off again and a final zero-ozone data point was measured at the 0 cm position. For every filter sample $[BaP]_S$ was calculated as described above, and the relative standard deviation of the three samples collected for one data point was typically 5%. The total duration of a single kinetic measurement run was several hours, and some runs exhibited a systematic drift of $[BaP]_{S,0}$ indicated by a significant difference between the initial and final zero-ozone data points. This difference was usually less than 10% but in a few cases increased up to 20% and was corrected by interpolation.

For the corrected data points $[BaP]_S/[BaP]_{S,0}$ was plotted on a logarithmic scale against reaction time, which was calculated as described in the Experimental Section. Figure 3 shows five representative measurement runs at different ozone VMRs under dry conditions. The data points and error bars represent the mean and standard deviation (±1 s.d.) of the triplicate sampling and analysis performed at every sampling position. The linearity of the BaP decays clearly demonstrates that the reaction is first-order with respect to BaP, and for every measurement run a pseudo-first-order rate coefficient $k_{1,m}$ was determined from the slope of linear least-squares fits like the ones shown in Figure 3. The mean rate coefficient of six measurement runs performed at zero ozone concentration was $k_{1,w} = (4 \pm 6) \times 10^{-4}$ s^{-1}. $k_{1,w}$ represents the minor decay of BaP by processes not related to ozone (e.g., particle wall loss) and was subtracted from $k_{1,m}$ to obtain a corrected rate coefficient k_1, which describes the actual reaction of BaP with ozone and is used for all further calculations ($k_1 = k_{1,m} - k_{1,w}$). In Figure 4 the corrected pseudo-first-order rate coefficients k_1 of all kinetic measurement runs performed under standard experimental conditions are plotted against the ozone concentration in the flow tube. The error bars represent the standard errors of the linear least-squares fits (±1 s.e.), ranging between ∼5% for the steeper slopes at high ozone and 10−20% for small slopes at low ozone. Clearly the rate coefficients increased less than linearly with $[O_3]$ and were reduced under humid conditions. The dependence of k_1 on ozone and water vapor concentration and the fit curves displayed in Figure 4 will be discussed below.

Additional kinetic measurement runs with the different initial BaP surface coverages listed in Table 1 were performed at an ozone VMR of (300 ± 2) ppb under dry conditions. For submonolayer surface coverages ($\theta_{BaP,0} < 1$) the observed rate coefficient exhibited no significant dependence on $\theta_{BaP,0}$, but at $\theta_{BaP,0} = 2$ it was 30% lower. Obviously BaP molecules right at the surface, which are directly exposed to gaseous ozone, are degraded significantly faster than molecules which are covered by other BaP molecules or reaction products. Thus, the observation of a reduced reaction rate at $\theta_{BaP,0} = 2$ is also consistent with the BaP surface coverage calculations.

Gas-Phase Ozone Loss. As described above, no significant gas-phase ozone loss was observed during the BaP degradation kinetics measurement runs, i.e., $[O_3]$ was independent of sampling position and reaction time. However, reproducible changes of $[O_3]$ could be observed in experiments where the spark discharge aerosol generation was switched on and off while all other conditions were kept constant. Such experiments were performed for different ozone VMRs, BaP surface coverages, and particle number concentrations under dry and humid conditions. The ozone VMRs and particle number concentrations measured in one of these experiments are shown in Figure 5.

When the spark discharge was switched off, the particle concentration exhibited an exponential decay with an e-folding time of ∼50 s, while the ozone VMR increased and reached an elevated steady-state value after ∼300 s. When the particle generation was turned on again, the particle concentration increased sharply, reaching steady-state after ∼50 s, while the ozone VMR decreased and reached a lower steady-state value again after ∼300 s. With respect to instrument specifications, sampling tube volumes and sampling flows the ozone and particle number concentration measurements should have had similar response times of 10−15 s. The delayed response of the observed ozone VMR to particle concentration changes was apparently due to equilibration effects between the gas phase and the walls of the tubing and UV absorption measurement cell (ozone adsorption/desorption).

The actual interaction time between gas-phase ozone and soot aerosol particles before measurement was ∼15 s in most ozone loss experiments (sampling right after the ozone mixing nozzle

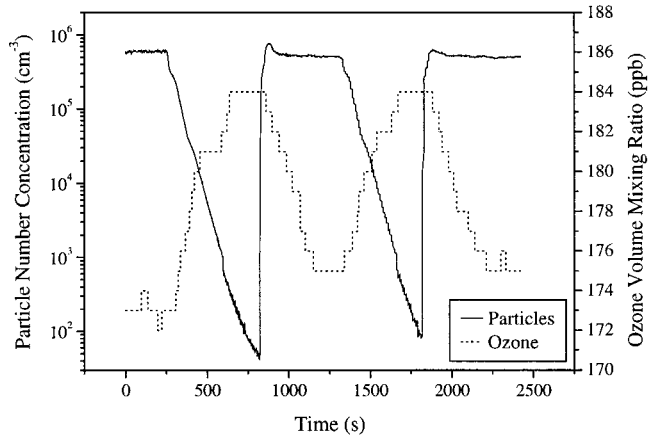

Figure 5. Representative measurement of particle-related ozone loss under dry conditions and with BaP-coated spark discharge soot particles ($\theta_{BaP,0} = 2$). Particle number concentration and ozone volume mixing ratio monitored at the flow tube entrance are plotted against the duration of the experiment, in which the spark discharge soot generator was twice switched off and on again.

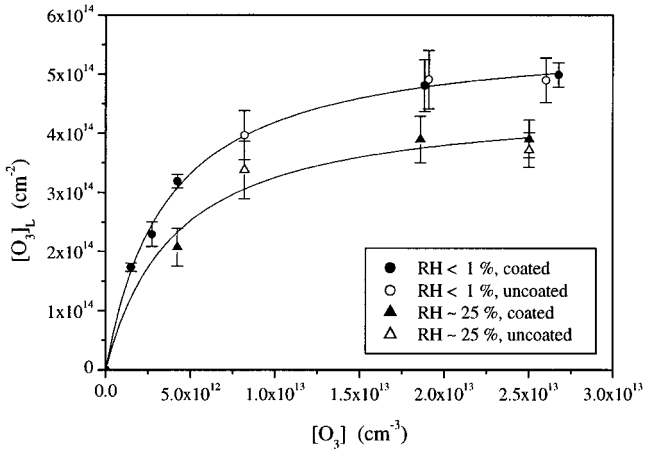

Figure 6. Particle-related gas-phase ozone loss as a function of gas-phase ozone concentration. The number of gas-phase ozone molecules lost per unit particle surface area is plotted against gas-phase ozone concentration. The upper data set was measured under dry conditions, the lower one at 25% relative humidity. The full and open symbols stand for BaP-coated and uncoated spark discharge soot particles, respectively. The data points and error bars represent the means and standard deviations (± 1 s.d.) of 4−6 consecutive measurements. The curves are nonlinear least-squares fits based on Langmuir adsorption isotherms (eqs 10 and 16).

at the flow tube entrance). Test experiments with ~50 s interaction time (sampling position 50 cm) yielded no significantly different results, which implies that the gas-phase ozone loss occurred on a shorter time scale than the BaP decay, as discussed below.

For every switching of the aerosol generator, the number of gas-phase ozone molecules lost per unit particle surface area $[O_3]_L$ was calculated as the ratio between the steady-state difference of $[O_3]$ and the corresponding difference of particle number concentration multiplied by the average particle surface area S_p. In Figure 6 $[O_3]_L$ is plotted against $[O_3]$. Every data point represents an average of 4 to 6 values from consecutive measurements in which the spark discharge was switched on or off, and the error bars represent the standard deviation (±1 s.d.). Full and open symbols stand for experiments with and without BaP coating on the soot aerosol particles, respectively. In the experiments with coated particles the BaP surface coverage was varied between 0.2 and 2 monolayers (T_{BaP} = 353 or 373 K). The results clearly show that the gas phase ozone loss was not significantly affected by BaP, i.e., $[O_3]_L$ was practically the same on coated and uncoated particles. In a similar way as the BaP decay rate coefficient, $[O_3]_L$ increased less than linearly with $[O_3]$ and was reduced under humid conditions. The dependence of $[O_3]_L$ on gas-phase ozone and water vapor concentration and the fit curves displayed in Figure 6 will be discussed below.

Mechanistic Interpretation. The simplest possible mechanistic interpretation of the heterogeneous reaction between ozone and benzo[*a*]pyrene on soot is an elementary bimolecular collision process. The rate of such an elementary reaction, r_e (cm^{-2} s^{-1}), could be described by

$$r_e = k_{2,eff}\,[O_3]\,[BaP]_S \tag{1}$$

and thus the pseudo-first-order rate coefficient for the BaP decay would be given by

$$k_1 = k_{2,eff} \tag{2}$$

According to the rule of additivity of kinetic resistances, the effective second-order rate coefficient $k_{2,eff}$ can be split into a collisional reaction rate coefficient $k_{2,c}$ and a diffusion-limited rate coefficient $k_{2,d}$:[1,32,33]

$$\frac{1}{k_{2,eff}} = \frac{1}{k_{2,c}} + \frac{1}{k_{2,d}} \tag{3}$$

On the basis of gas kinetic theory $k_{2,c}$ can be related to a reaction probability γ_{BaP}, which is defined as the fraction of collisions between O_3 gas molecules and BaP surface molecules that leads to reactive loss of BaP ($0 \le \gamma_{BaP} \le 1$):

$$k_{2,c} = \frac{\gamma_{BaP}\sigma_{BaP}\omega_{O_3}}{4} \tag{4}$$

σ_{BaP} is the cross section of the BaP surface molecules, and ω_{O_3} is the mean thermal velocity of ozone molecules given by $[8RT/(\pi M_{O_3})]^{1/2}$, where R stands for the gas constant, T is the absolute temperature and M_{O_3} is the molar mass of ozone ($\omega_{O3} = 3.61 \times 10^4$ cm s^{-1} at 296 K). On the basis od Fick's law and assuming spherical geometry for the aerosol particles, the diffusion-limited rate coefficient can be derived from the maximum flux to a spherical surface:[34]

$$k_{2,d} = \frac{\sigma_{BaP}D_{O_3}}{r_p} \tag{5}$$

D_{O_3} stands for the gas-phase diffusion coefficient of ozone, and r_p is the particle radius.

In contrast to the linear relation between k_1 and $[O_3]$ suggested by the above definitions and equations, the observed pseudo-first-order rate coefficients do not exhibit a linear increase with ozone (Figure 4). Thus, the heterogeneous reaction between O_3 and BaP on soot does not represent an elementary bimolecular collision process with a concentration-independent reaction probability. However, also apparent reaction probabilities, which are just proportionality factors between heterogeneous reaction rates and gas kinetic surface collision fluxes rather than basic physicochemical parameters, are illustrative and frequently used in atmospheric research. Thus, an apparent reaction probability γ_{BaP} was calculated for every experimental data pair of k_1 and

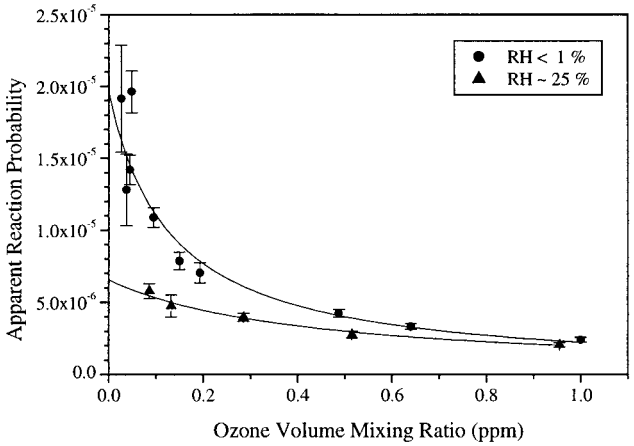

Figure 7. Apparent BaP−O_3 reaction probability as a function of ozone volume mixing ratio. The upper data set was calculated from the pseudo-first-order BaP decay rate coefficients observed under dry conditions, the lower one from those observed at 25% relative humidity. The error bars correspond to the standard errors of the pseudo-first-order rate coefficients (±1 s.e.). The curves are to guide the eye (nonlinear least-squares fits based on eqs 6 and 9).

$[O_3]$ based on eqs 2−5. Assuming $\sigma_{BaP} = 1$ nm[2,30] $D_{O_3} = 0.2$ $cm^2\ s^{-1}$ (estimated according to the Fuller method)[35] and $r_p =$ 60 nm (mobility equivalent radius of average surface area), a value of 3×10^{-10} $cm^3\ s^{-1}$ was obtained for $k_{2,d}$. Since $1/k_{2,d}$ is several orders of magnitude smaller than all experimental values of $1/k_{2,eff} = [O_3]/k_1$, the effect of gas-phase diffusion on the rate of the investigated heterogeneous reaction is negligible, regardless of the actual reaction mechanism. In Figure 7 apparent reaction probabilities calculated according to

$$\gamma_{BaP} = \frac{4}{\sigma_{BaP}\omega_{O3}}\frac{k_1}{[O_3]} \tag{6}$$

are plotted versus ozone VMR. With increasing ozone γ_{BaP} decreased from about 2×10^{-5} to 2×10^{-6} under dry conditions (RH < 1%) and from 6×10^{-6} to 2×10^{-6} under humid conditions (RH ∼ 25%). The error bars correspond to the standard errors of the pseudo-first-order rate coefficients (±1 s.e.). The two curves are to guide the eye and were obtained by nonlinear least-squares fits based on eqs 6 and 9.

The shape of the k_1 vs $[O_3]$ plots displayed in Figure 4 is similar to an adsorption isotherm and suggests a multistep reaction mechanism involving reversible adsorption of ozone at the particle surface. Also the plots of $[O_3]_L$ vs $[O_3]$ displayed in Figure 6 suggest reversible ozone adsorption according to a simple Langmuir isotherm. Thus, the most straightforward interpretation of the observed BaP decay rates consists of a quickly established adsorption equilibrium followed by a much slower bimolecular surface reaction between adsorbed ozone and BaP as the rate-limiting step. In this case the overall BaP decay rate equals the surface reaction rate, r_S ($cm^{-2}\ s^{-1}$), given by

$$r_S = k_{2,S}\,[O_3]\,[BaP] \tag{7}$$

$k_{2,S}$ is a second-order surface reaction rate coefficient, and the surface concentration of adsorbed ozone molecules $[O_3]_S$ can be regarded as the product of the surface concentration of ozone adsorption sites $[SS]_S$ and the ozone surface coverage θ_{O_3}: $[O_3]_S = [SS]_S\theta_{O_3}$. Assuming a Langmuir isotherm, the ozone surface coverage is given by

$$\theta_{O_3} = \frac{K_{O_3}[O_3]}{1 + K_{O_3}[O_3]} \tag{8}$$

K_{O_3} is the Langmuir adsorption equilibrium constant for ozone, i.e., the ratio between the ozone adsorption and desorption rate coefficients $k_{a,O_3}/k_{d,O_3}$ (see below). On the basis of eqs 7 and 8 the pseudo-first-order rate coefficient of the observed BaP decay, k_1 can be interpreted as

$$k_1 = \frac{k_{2,S}[SS]_S K_{O_3}[O_3]}{1 + K_{O_3}[O_3]} \tag{9}$$

For a constant value of $[SS]_S$, the product $k_{2,S}$ $[SS]_S$ represents the maximum pseudo-first-order BaP decay rate coefficient in the limit of high ozone concentrations ($\theta_{O_3} \rightarrow 1$), $k_{1,\infty}$. A nonlinear least-squares fit of eq 9 (with $k_{2,S}[SS]_S = k_{1,\infty}$) to the experimental data pairs of k_1 and $[O_3]$ under dry conditions is displayed in Figure 4 (upper curve), the fit parameters are summarized in Table 2. For the adsorption equilibrium constant K_{O_3} and for the maximum pseudo-first-order rate coefficient $k_{1,\infty}$, values of 2.7×10^{-13} cm^3 and 0.015 s^{-1}, respectively, were obtained.

Provided that the irreversible loss of ozone by chemical reaction is negligible against the gas-phase ozone loss by reversible adsorption, which will be discussed below, $[O_3]_S$ can be approximated by $[O_3]_L$ which leads to the equation

$$[O_3]_L = \frac{[SS]_S K_{O_3}[O_3]}{1 + K_{O_3}[O_3]} \tag{10}$$

A nonlinear least-squares fit of eq 10 to the experimental data pairs of $[O_3]_L$ and $[O_3]$ under dry conditions is displayed in Figure 6 (upper curve), and the fit parameters are summarized in Table 2. $K_{O_3} = 2.8 \times 10^{-13}$ cm^3 is in excellent agreement with the fit of eq 9 to the observed BaP decay rate coefficients, and for $[SS]_S$ a value of 5.7×10^{14} cm^{-2} was obtained. From $k_{1,\infty}$ and $[SS]_S$ follows $k_{2,S} = 2.6 \times 10^{-17}$ $cm^2\ s^{-1}$.

In a simple model based on Langmuir adsorption and gas kinetic theory, the rate of adsorption, r_{a,O_3} ($cm^{-2}\ s^{-1}$), should be proportional to the collision rate of gas-phase ozone molecules with the surface, which can be approximated by $[O_3]\omega_{O_3}/4$, to the sticking probability of ozone at the clean surface without occupied adsorption sites S_{0,O_3}, and to the actual fraction of unoccupied adsorption sites, $1 - \theta_{O_3}$.[34]

$$r_{a,O_3} = \frac{S_{0,O_3}\omega_{O_3}}{4}[O_3](1 - \theta_{O_3}) \tag{11}$$

Here the sticking probability S_{0,O_3} ($0 \le S_{0,O_3} \le 1$) is defined as the ratio between the adsorption rate and the surface collision rate of ozone at $\theta_{O_3} = 0$. Relations and definitions for the sticking probability and similar terms like sticking coefficient, mass accommodation coefficient, uptake coefficient, etc., which are frequently used in slightly different ways and contexts, as well as corrections of the surface collision rate in the case of high net uptake of gas molecules at the surface, have been described in detail elsewhere.[1,33,34,36] The rate of desorption, r_{d,O_3} ($cm^{-2}\ s^{-1}$), should be proportional to the surface concentration of adsorbed ozone molecules $[SS]_S\theta_{O_3}$, and to the inverse of their mean residence time at the surface τ_{O_3}:

$$r_{d,O_3} = \frac{[SS]_S}{\tau_{O_3}}\theta_{O_3} \tag{12}$$

TABLE 2: Langmuir Adsorption Equilibrium Constants, Adsorption Site Surface Concentrations, and Maximum Pseudo-First-Order BaP Decay Rate Coefficients Obtained from the Curve Fits Displayed in Figures 4 and 6

Data Set	K_{O_3} (10^{-13} cm^3)	K_{H_2O} (10^{-17} cm^3)	$[SS]_S$ (10^{14} cm^{-2})	$k_{1,\infty}$ (s^{-1})	R^2	n
k_1 vs $[O_3]$, dry	2.7 ± 0.4 (1.9−4.0)			0.015 ± 0.001 (0.013−0.017)	0.972	11
$[O_3]_L$ vs $[O_3]$, dry	2.8 ± 0.2 (2.4−3.2)		5.7 ± 0.1 (5.5−5.9)		0.997	9
k_1 vs $[O_3]$, humid		2.1 ± 0.4 (1.2−3.5)		0.016± 0.001 (0.013−0.019)	0.995	6
$[O_3]_L$ vs $[O_3]$, humid		0.1 ± 0.3 (0−1.3)	4.6 ± 0.3 (3.8−5.6)		0.980	6
preferred values	2.8 ± 0.2 (2.4−3.2)	2.1 ± 0.4 (1.2−3.5)	5.7 ± 0.1 (5.5−5.9)	0.015 ± 0.001 (0.013−0.017)		

[a] The nonlinear least-squares fits based on eqs 9, 10, 15, and 16 were performed using a Levenberg−Marquardt algorithm (Origin 6.0 data analysis software). The best-fit values are given together with their standard errors and with the upper and lower limits of their 95% confidence intervals (in parentheses). Note that for $[SS]_S$ the statistical standard errors are much smaller than the overall error estimate (see discussion). The last two columns indicate the goodness-of-fit (R^2) and the number of data points (n). The preferred values for the physicochemical parameters are summarized in the last line (narrowest confidence interval, highest R^2 and n).

According to eqs 10 and 11, the adsorption and desorption rate coefficients can be defined as $k_{a,O_3} = S_{0,O_3}\omega_{O_3}/4$ and $k_{d,O_3} = \tau_{O_3}^{-1}$ $[SS]_S$, and for the Langmuir equilibrium constant follows

$$K_{O_3} = \frac{S_{0,O_3}\omega_{O_3}}{4\,[SS]_S}\,\tau_{O_3} \tag{13}$$

In several previous studies with spark discharge soot, as well as with other soot model substances, values of about 1.0×10^{-3} to 3.3×10^{-3} have been determined for S_{0,O_3}.[37−39] This was confirmed by the results of our gas-phase ozone loss experiments, since a sticking coefficient on the order of 10^{-3} or larger is required to establish the observed time-independence, i.e., to saturate 5.7×10^{14} adsorption sites per cm^2 within the minimum experimental ozone-soot interaction time of ∼15 s. With $K_{O_3} = 2.8 \times 10^{-13}$, $[SS]_S = 5.7 \times 10^{14}$ cm^{-2}, and $S_{0,O_3} = 1.0 \times 10^{-3}$ a mean residence time of 18 s was calculated for O_3 at the surface of the investigated aerosol particles ($\tau_{O_3} = 5$ s for $S_{0,O_3} = 3.3 \times 10^{-3}$). The relatively long residence time and the fact that the experimental data can be described by a Langmuir isotherm suggest chemisorption rather than physisorption. Assuming an Arrhenius−type temperature dependence of k_{d,O_3} with a preexponential factor on the order of 10^{14} s^{-1}, which is typical for chemisorbed species,[34] an estimate of 90 kJ mol^{-1} (80 kJ mol^{-1} for $\tau_{O_3} = 5$ s) can be calculated for the negative adsorption enthalpy. This is clearly higher than the 20−50 kJ mol^{-1} usually observed for physisorption processes.[34]

The slower decay of BaP and the smaller gas-phase ozone loss observed under humid conditions indicate that the adsorption of ozone is inhibited by competitive adsorption of H_2O at the aerosol particle surface. Assuming that the adsorption of water vapor can be described independently by a Langmuir isotherm with an equilibrium constant K_{H_2O}, the ozone surface coverage under humid conditions is given by

$$\theta_{O_3} = \frac{K_{O_3}[O_3]}{1 + K_{O_3}[O_3] + K_{H_2O}\,[H_2O]} \tag{14}$$

$[H_2O]$ is the water vapor concentration, and for the pseudo-first-order rate coefficient of the BaP decay follows

$$k_1 = \frac{k_{2,S}[SS]_S K_{O_3}[O_3]}{1 + K_{O_3}[O_3] + K_{H_2O}[H_2O]} \tag{15}$$

A nonlinear least-squares fit of eq 15 (with $k_{2,S}\,[SS]_S = k_{1,\infty}$) to the experimental data pairs of k_1 and $[O_3]$ under humid conditions is displayed in Figure 4 (lower curve). With $K_{O_3} = 2.8 \times 10^{-13}$ cm^3 and $[H_2O] = 1.7 \times 10^{17}$ cm^{-3} (25% RH at 296 K), values of 2.1×10^{-17} cm^3 and 0.016 were obtained for K_{H_2O} and $k_{1,\infty}$, respectively (Table 2). With $K_{O_3} = 2.7 \times 10^{-13}$ cm^3 the results were practically the same. The excellent agreement of $k_{1,\infty}$ under dry and humid conditions supports the idea that water vapor interferes by competitive adsorption rather than in the actual surface reaction between O_3 and BaP.

In analogy to eq 10, a nonlinear least-squares fit to the experimental data pairs of $[O_3]_L$ and $[O_3]$ under humid conditions was performed with the following equation and is displayed in Figure 6 (lower curve):

$$[O_3]_L = \frac{[SS]_S K_{O_3}[O_3]}{1 + K_{O_3}[O_3] + K_{H_2O}[H_2O]} \tag{16}$$

With $K_{O_3} = 2.8 \times 10^{-13}$ cm^3 and $[H_2O] = 1.7 \times 10^{17}$ cm^{-3} values of 0.1×10^{-17} cm^3 and 4.6×10^{14} cm^{-2} were obtained for K_{H_2O} and $[SS]_S$, respectively (Table 2). Again the results were not significantly different with $K_{O_3} = 2.7 \times 10^{-13}$ cm^3. The agreement of the values obtained for K_{H_2O} and $[SS]_S$ from the fit of eq 16 with the values from eqs 15 and 10, respectively, is not as good as for the independent determinations of K_{O_3} and $k_{1,\infty}$ (eqs 9, 10, and 15). However, also for K_{H_2O} and $[SS]_S$ the 95%-confidence intervals given in Table 2 show an overlap.

In analogy to eq 13, K_{H_2O} can be related to the mean residence time of water molecules on the ozone adsorption sites at the particle surface τ_{H_2O}:

$$K_{H_2O} = \frac{S_{0,H_2O}\omega_{H_2O}}{4\,[SS]_S}\,\tau_{H_2O} \tag{17}$$

S_{0,H_2O} is the sticking coefficient, and ω_{H_2O} is the mean thermal velocity of water vapor molecules ($\omega_{H_2O} = 5.90 \times 10^4$ cm s^{-1} at 296 K). With commercial carbon black as a soot model substance a value of 0.4×10^{-3} has been determined for S_{0,H_2O}, which was found to be the same for ozone treated and untreated samples.[39] With $K_{H_2O} = 2.1 \times 10^{-17}$ cm^3, $[SS]_S = 5.7 \times 10^{14}$ cm^{-2}, and $S_{0,H_2O} = 0.4 \times 10^{-3}$ a mean residence time of 3×10^{-3} s was calculated for H_2O on the ozone adsorption sites of the investigated aerosol particles.

The relatively short residence time and the fact that BaP coated and uncoated spark discharge soot particles are known to be rather hydrophobic[5,12] suggest physisorption rather than chemisorption of water vapor. Again assuming an Arrhenius−

type temperature dependence for k_{d,H_2O} with a preexponential factor on the order of 10^{12} s^{-1}, which is typical for physisorbed species,[34] an estimate of 50 kJ mol^{-1} can be calculated for the negative adsorption enthalpy. This is compatible with the maximum negative enthalpy of 57 kJ mol^{-1} reported for the physisorption of H_2O.[34]

Discussion

The mechanism proposed above for the heterogeneous reaction of ozone with benzo[*a*]pyrene on spark discharge soot particles is supported by all experimental findings. The assumption that a reversible adsorption equilibrium is quickly established while the subsequent surface reaction represents the rate-limiting step was confirmed by the observation that the gas-phase ozone loss occurs on a shorter time scale than the BaP decay ($S_{0,O_3} \geq 10^{-3}$, $\gamma_{BaP} \leq 2 \times 10^{-5}$) as well as by the high goodness-of-fit obtained with eqs 9, 10, 15, and 16 which are based on Langmuir isotherms (Figures 4 and 6, Table 2). From the four data sets two independent estimates were determined for every fit parameter (Table 2). The two values obtained for K_{O_3} and $k_{1,\infty}$ obtained from eqs 15, 10, and 9 are more or less identical. Because of the narrower 95%-confidence intervals $K_{O_3} = 2.8 \times 10^{-13}$ cm^3, and $k_{1,\infty} = 0.015$ s^{-1} will be used preferentially. Only the values for K_{H_2O} and $[SS]_S$ obtained from the fit of eq 16 to the data set with the lowest statistical quality ($[O_3]_L$ vs $[O_3]$ under humid conditions) were significantly different from the values obtained with the other equations and data sets. However, also in this case the 95%-confidence intervals show an overlap. Again the estimates with narrower confidence intervals are preferred: $K_{H_2O} = 2.1 \times 10^{-17}$ cm^3 and $[SS]_S = 5.7 \times 10^{14}$ cm^{-2}. In addition to the above results also the close agreement of $[O_3]_L$ measured with BaP coated and uncoated particles supports the assumption of a constant surface concentration of ozone adsorption sites, $[SS]_S$, at least on the experimental time scale of a few seconds to minutes.

Since there is no indication of significant systematic errors affecting the measurement of k_1 and $[O_3]$, the statistical standard errors given in Table 2 can be regarded as appropriate overall error estimates for the parameters derived from the k_1 vs $[O_3]$ data sets ($k_{1,\infty}$, K_{O3}, and K_{H_2O}). $[O_3]_L$ and the parameters derived from the $[O_3]_L$ vs $[O_3]$ data sets ($[SS]_S$ and $k_{2,S}$), however, are subject to a potential systematic error on the order of $\pm$ 30%, corresponding to the error limits estimated for the average particle surface area used for the calculation of $[O_3]_L$.

Gas-Phase Ozone Loss. If the surface structure of the uncoated spark discharge soot particles is assumed to resemble a graphite layer or a large polycyclic aromatic hydrocarbon, it consists primarily of condensed six-membered carbon rings with a surface concentration of 1.9×10^{15} cm^{-2}.[15] Similarly the surface of the coated particles with $\theta_{BaP} \geq 1$ can be pictured as a layer of $\sim 10^{14}$ BaP molecules per cm^{-2}, each of which provides five fused aromatic rings and 12 adjacent "gaps" of similar geometry framed by carbon and hydrogen atoms amounting to a total of $\sim 1.7 \times 10^{15}$ potential adsorption sites per cm^{-2}. As pointed out above, the gas-phase ozone loss was the same in both cases, and $[SS]_S = 5.7 \times 10^{14}$ cm^{-2} implies that up to one-third of the carbon rings and "gaps" can be occupied by ozone.

Similar observations were reported by Kamm et al.[15] from aerosol chamber experiments with ozone and uncoated spark discharge soot. Assuming an accessible specific surface of only ~ 200 m^2 g^{-1}, they determined a value of 6.5×10^{14} cm^{-2} for the number of gas phase ozone molecules rapidly lost per unit surface area at an ozone VMR of 100 ppb. On the other hand a lower value of 3×10^{14} cm^{-2} at 915 ppb O_3 can be derived from the data published by Fendel et al.[22] who performed aerosol flow tube experiments with ozone and uncoated spark discharge soot.

In both of these studies, however, the observed gas-phase ozone loss was described as an irreversible process, initialized by the adsorption of an oxygen atom and liberation of molecular oxygen rather than by reversible adsorption of an ozone molecule. In this picture the adsorption of O atoms was followed either by a catalytic reaction in which the adsorbed O atoms react with each other or with gas-phase O_3 to form O_2, or by surface oxidation which leads to a rate-limiting desorption of CO/CO_2 or to a surface passivation.[15,22] Also Smith and Chughtai[40] postulated a fast catalytic decomposition of ozone on fresh *n*-hexane soot surfaces, followed by the formation of oxygen containing functional groups at the soot surface involving physisorbed O_2 molecules, by the release of CO_2 and H_2O, and by further ozone loss which is second-order in $[O_3]$ and involves chemisorbed O atoms. Longfellow et al.[16] recently reported results of ozone uptake measurements on hydrocarbon soot, which were consistent with the data and interpretation of Smith and Chughtai.[40]

In contrast, Stephens et al.[37] interpreted their results from Knudsen cell measurements with ozone and ground charcoal in a similar way as proposed in the preceding section. They suggested that ozone molecules are reversibly adsorbed according to a Langmuir isotherm with an initial sticking coefficient of 10^{-3} and subsequently undergo a slow surface reaction in which surface carbonyl groups, CO and CO_2 are formed. However, they did not attempt to estimate adsorption equilibrium constants or enthalpies. They reported that after exposing the sample to an ozone dose equivalent to a monolayer of adsorbed O_3, which would be on the order of $(1-2) \times 10^{14}$ cm^{-2} according to their data, the ozone loss proceeded at slow steady-state rates characterized by effective sticking coefficients or reaction probabilities on the order of $10^{-4}-10^{-5}$. From the kinetic parameters published by Kamm et al.,[15] effective reaction probabilities on the order of $10^{-6}-10^{-7}$ can be calculated for the loss of ozone on spark discharge soot on a time scale of minutes to a few hours (1×10^{-6} at 100 ppb O_3 decreasing to 3×10^{-7} at 1000 ppb O_3).

The apparent reaction probabilities for the degradation of BaP on spark discharge soot by ozone determined in this work, $\gamma_{BaP} \sim 10^{-5}-10^{-6}$, lie right in the middle of the above range of effective reaction probabilities for the loss of ozone on various types of soot. Considering our experimental results in combination with those of the previous studies, we support the interpretation by Stephens et al.[37] and extend it proposing the following mechanistic hypothesis: On fresh soot covered with PAH or small domains of graphite-like carbon layers on the order of a few nm[2,41] reversible adsorption leads to a fast initial gas-phase ozone loss characterized by a sticking coefficient on the order of 10^{-3}. Further irreversible ozone loss occurs primarily via oxidation of the surface PAH or carbon layers, which leads to the formation of oxygen-containing functional groups (carbonyl, hydroxyl, carboxyl, etc.).[1,42] At first this oxidation process is expected proceed at similar or somewhat slower rates than the observed BaP decay (apparent reaction probability $10^{-5}-10^{-6}$), since BaP is generally regarded as one of the more reactive PAH.[1] Further oxidation of the partially oxidized polycyclic aromatics or carbon layers proceeds at significantly slower rates and eventually leads to the formation of CO/CO_2 and (semi)volatile organics.

In parallel to the oxidation processes also a catalytic decomposition of ozone may occur on the particle surface. However, already Stephens et al.[37] stated explicitly that their results did not point toward a catalytic mechanism. Kamm et al.[15] included a very slow catalytic reaction in parallel to the surface oxidation process in their mechanism, but pointed out that they did not expect their mechanism to be correct on a molecular level. Also the rapid initial ozone loss, which Smith and Chughtai[40] attributed to catalytic decomposition, may in fact be due to reversible ozone adsorption, which may in addition account for the apparent excess formation of oxidation products they tentatively explained by O_2 adsorption. To definitively answer the question whether catalytic ozone destruction on graphite-like or PAH-coated surfaces at sub-ppm of O_3 levels is important or negligible compared to the gas-phase ozone loss by reversible adsorption and subsequent oxidation processes, additional investigations will be needed. Nevertheless, we think that the results available up to now rather point toward a negligible role of catalytic mechanisms.

The experimental findings of our study and of the previous investigations do not allow an unambiguous distinction whether intact ozone molecules or oxygen atoms as an alternative form of "odd oxygen" are adsorbed at the particle surface. However, the negative adsorption enthalpy of 80−90 kJ mol^{-1} derived from the observed adsorption equilibrium constant is smaller than the ozone dissociation enthalpy of 106.5 kJ mol^{-1} and does not suggest the cleavage of O_3 upon adsorption. Moreover one may expect higher BaP decay rates if indeed oxygen atoms, which have a higher oxidizing power than ozone, were adsorbed on the particle surface and BaP molecules, respectively. In any case also the adsorption of O atoms would have to be reversible in order to explain the Langmuir-type behavior of the gas-phase ozone loss and BaP decay rates measured in this work. Additional experiments to discriminate between ozone molecules and O atoms on the surface are in preparation.

For the half-life of adsorbed O_3 (or O atoms) with respect to chemical reaction with BaP an estimate of 270 s can be calculated by inserting $k_{2,\infty} = 2.6 \times 10^{-17}$ cm^2 s^{-1} and $[BaP]_S = 1 \times 10^{14}$ cm^{-2} as the maximum concentration of BaP at the surface (monomolecular layer) into eq 7. This is by a factor of 15−54 longer than the mean residence time of 5−18 s calculated above and consistent with the assumption of a quickly established adsorption equilibrium followed by a much slower surface reaction.

Neither for the adsorption enthalpy nor for the mean residence time of ozone on PAH− or graphite-like surfaces a literature reference value is known to the authors. The mean residence time calculated for H_2O, however, is in excellent agreement with the results of a recent study by Alcala-Jornod and Rossi.[43] They performed uptake experiments in a diffusion tube and determined values of 0.1−5 ms for τ_{H_2O} on decane, toluene, diesel and acetylene soot samples by Monte Carlo trajectory model calculations. Moreover the Langmuir adsorption equilibrium constants determined in the present study for H_2O on spark-discharge soot particles with or without BaP coating (Table 2, preferred value: $K_{H_2O} = 2.1 \times 10^{-17}$ cm^3 = 0.51 mbar^{-1} = 12.6 L mmol^{-1}) are of the same order of magnitude as the Langmuir adsorption equilibrium constants recently reported for H_2O on self-assembled monolayers of C_8−C_{18} alkanes and alkenes (0.10−0.27 mbar^{-1} and 2.3−6.1 L mmol^{-1}).[44,45]

Since no significant difference was observed for the gas-phase ozone loss and its reduction by water vapor on BaP-coated and -uncoated spark discharge soot, the adsorption equilibrium constants K_{O_3} and K_{H_2O} as well as the mean residence times τ_{O_3} and τ_{H_2O} are apparently the same on spark discharge soot as on BaP and most probably also on other PAH. Moreover the consistency of our findings with most experimental results of the studies discussed above suggests that the presented mechanistic picture of rapid, reversible, and competitive adsorption followed by slow surface oxidation can also be applied for the interaction of gaseous ozone and water vapor with particles consisting of other graphite-, charcoal-, or soot-like materials and supports the suitability of PAH/PAC as model substances for these materials and for the refractory core of real soot particles. Note that even the ozone removal efficiency of the activated-carbon diffusion denuders used in the reaction system was consistent with this picture. It was reversibly reduced by a few percent in the experiments under humid conditions and decreased slowly with increasing accumulated exposure to ozone.

On the other hand carbonaceous combustion aerosol particles coated with organic or aqueous liquid layers (e.g., wood smoke particles)[1] can of course interact differently with ozone, since in this case O_3 can not only be adsorbed at the surface but as well diffuse into the liquid layer and react with different aliphatic, aromatic, and inorganic components.

Benzo[*a*]pyrene Degradation Kinetics. Obviously the existence and composition of liquid surface layers as described above can also influence the reactivity of BaP on aerosol particles. The following considerations, however, are focused on the degradation kinetics of BaP deposited on different solid substrates and exposed to gaseous ozone. In several previous studies results ranging from zero reactivity to half-lives on the order of 30−60 min at 200 ppb O_3 or ∼15 min at 1 ppm of O_3 have been reported,[1,4] and only in a few cases similarly high BaP decay rate coefficients were measured as in this work.[46−49] To explain the wide range of results mainly two potential reasons have been discussed: (a) surface/bulk shielding effects physically limiting the interaction of bulk molecules with gas-phase ozone and (b) chemical activation or passivation of BaP surface molecules by interaction with their substrate.

Wu et al.[46] already pointed out that well-dispersed BaP molecules reacted much faster than the BaP molecules in aggregated clusters or multilayers. In agreement with our interpretation of the significantly reduced decay rate we observed at $\theta_{BaP} = 2$ relative to $\theta_{BaP} \leq 1$, they attributed the slower reaction of the bulk material to the formation of a surface layer of oxidation products, which do not leave the surface but act as a diffusion barrier hindering the access of ozone to the bulk. On the other hand they reported a first-order dependence of the BaP decay rate on ozone VMR over the range from 0 to 1.5 ppm ($k_2 = 0.022$ s^{-1} ppm^{-1}), which suggests an elementary collision process with a reaction probability of 1.0×10^{-5} rather than the Langmuir-adsorption process observed in this work. This discrepancy can be explained either by really different reaction mechanisms, which are caused by the different BaP substrates but nevertheless lead to BaP decay rates of the same order of magnitude, or by experimental and interpretative artifacts.

The adsorption mechanism proposed above is supported by the independent gas-phase ozone loss measurements we performed as well as by the results of the other ozone loss studies mentioned before. The apparent first order dependence observed by Wu et al.,[46] however, may have been influenced by the following factors. The decrease of fluorescence intensity, which was used to determine the BaP decay rate, may have been caused not only by chemical degradation of BaP but also by reversible

adsorption of ozone on the BaP molecules. In fact the fast initial decay of signal intensity, which was used to calculate the rate coefficients, was not sustained throughout the measurement runs. Especially for the measurements at high ozone VMRs (1.0 and 1.5 ppm) the linearity of the initial decay plotted on a logarithmic scale seems to be restricted to the reaction time from zero to the first data point after 25 s only. This is not much more than the time required to establish an adsorption equilibrium if the sticking coefficient for O_3 on BaP and/or SiO_2 is similar as for O_3 on the soot-like materials described above. Since the decay of BaP was measured only at two more nonzero ozone VMRs (0.25 and 0.55 ppm) the apparent first-order dependence on $[O_3]$ may indeed have been a coincidental combination of chemical degradation and fluorescence quenching due to adsorption.

Alebic-Juretic et al.[48] investigated the reaction of ozone with BaP on silica gel particles suspended in a fluidized bed reactor. They also reported a first-order dependence of the BaP decay rate on ozone VMR over the range from 0 to 0.25 ppm and higher rate coefficients for sub-monomolecular surface layers: $k_2 = 0.008\ s^{-1}\ ppm^{-1}$ for $\theta_{BaP} < 1$ and $k_2 = 0.003\ s^{-1}\ ppm^{-1}$ for $\theta_{BaP} > 1$. They suggested that O_3 reacts only with the outer layer of BaP, but in contrast to Wu et al.[46] they assumed that the primary oxidation products would be rapidly blown off the surface and attributed the increased rate coefficients for submonolayer coverages to a chemical activation of BaP by the acidic silica gel surface.

However, the products which are formed in the first steps of oxidative BaP degradation have generally higher molecular weights and are more polar than BaP, which implies that they are less volatile. In product studies accompanying the kinetic experiments presented here, BaP quinones were found to be the main products of BaP degradation by ozone on spark discharge soot and glass fiber filter substrates, and a wide variety of other partially oxidized aromatics PAH have been detected as minor products (phenols, carboxylic acids, etc., with four or five condensed aromatic rings) but no strong blow-off effects were observed.[50,51] Since also pyrene-quinones, which are of considerably lower molecular mass than BaP quinones, were found to have slower sublimation rates than BaP on glass substrates,[47] the efficient blow-off of the oxidation products from the particle surface invoked by Alebic-Juretic et al.[48] appears to be highly improbable.

Also the postulated activation effect or reactivity enhancement of BaP by the silica gel surface[48,49] is not required to explain an apparent decrease of reaction rates at $\theta_{BaP} > 1$. Under the assumption that only surface BaP molecules can react with O_3, the apparent first-order rate coefficient describing the decay of the total amount of BaP (as measured after solvent extraction of the particles) has to decrease with increasing surface coverage for $\theta_{BaP} > 1$, which is easy to demonstrate by numerical simulation. This applies regardless of product volatility and holds true also if the bulk molecules can react with O_3 but at a much slower rate after diffusion through the surface layer of BaP and oxidation products or after further degradation and volatilization of the surface layer.

In any case the high reaction rates we observed for BaP on carbon particles, the surface of which is certainly less polar and acidic than that of silica gel, indicate that the acidity of the substrate does not significantly promote the reactivity of surface BaP molecules toward gaseous or adsorbed ozone. Not only the values reported by Alebic-Juretic et al.[48,49] but also the rate coefficient reported by Cope and Kalkwarf[47] for the reaction of O_3 with BaP on glass substrates ($0.002\ s^{-1}$ at 160 ppb O_3) was lower than the corresponding BaP decay rate coefficients observed in this work. If indeed the rate coefficients reported by Wu et al.[46] for O_3 + BaP on silica were overestimated due to the ozone adsorption and fluorescence quenching effects discussed above, the reaction rate of BaP with ozone actually appears to be reduced on silica and glass surfaces relative to graphite- or PAH-like surfaces.

The very limited set of measurement data points presented by Alebic-Juretic et al.[48] does not allow a closer investigation whether the discrepancy between the Langmuir-type behavior observed in this work and the apparent first-order dependence of the BaP decay on $[O_3]$ reported by Alebic-Juretic et al.[48] is due to different reaction mechanisms caused by the different substrates or to experimental or interpretative artifacts. Note, however, that the ozone VMRs investigated in their experiments are restricted to a range where also the Langmuir-type curves observed in this study exhibit a near-linear initial increase ($\leq$ 0.25 ppm of O_3). Thus, also the experimental results of Alebic-Juretic et al.[48,49] are not necessarily in contrast to the adsorption mechanism proposed above.

Regardless of the actual reaction mechanism, the fast BaP decay rates observed for submonolayer surface coverages on spark discharge soot particles, as well as on silica and glass substrates, indicate that even under dark conditions chemical aging leads to a rapid degradation of BaP surface molecules on any type of solid atmospheric particle. With the parameters given in Table 2, eq 15 can be used to estimate the lifetime of BaP molecules on PAH− or graphite-like surfaces with respect to the reaction with ozone at different relative humidities under ambient pressure and temperature (1 atm, 296 K). For example, in the presence of 30 ppb O_3 the estimated BaP half-life is only 4.5 min under dry conditions and increases significantly with relative humidity, reaching 18 min at 25% RH and 44 min at 75% RH.

The influence of humidity on the degradation of PAH by ozone has already been investigated in previous studies. Pitts et al.[52] exposed various PAH on glass fiber filter substrates at ambient temperature for 3 h to a gas flow containing ozone (200 ppb) and water vapor (1−50% RH). For pyrene, fluoranthene, benz[*a*]anthracene and benzo[*e*]pyrene they observed much less degradation at 50% RH (0−6% turnover) than at 1% RH (9−68% turnover). The differences were less pronounced on Teflon coated glass fiber filters but still accounted for a factor of 2 or more (22−58% vs 11−20% turnover). For BaP, however, they observed only a weak influence in both cases (50% vs 40% turnover). For atmospheric particle samples exposed to ozone in the same way, they observed a similar range of turnovers (0−70%) but no significant humidity effect. Thus, they attributed the influence of relative humidity to the adsorption of H_2O on the filter substrates rather than directly on the particles or PAH.

In contrast Kamens et al.[53] and McDow et al.[54] reported an increase of PAH degradation rates with increasing RH in experiments with wood smoke particles in outdoor Teflon film chambers exposed to sunlight. This reverse effect may be due to an enhancement of degradation pathways other than the reaction with ozone or to the influence of liquid surface layers. Wood smoke particles are generally assumed to be covered by a liquid organic layer[1,53] into which water as well as ozone can be dissolved rather than just being adsorbed at the surface.

Thus, the potential influence of liquid organic or aqueous layers on atmospheric particles has to be kept in mind when using the kinetic parameters presented in this work for extrapolations to the atmosphere. BaP molecules contained in the bulk

of liquid or solid particulate matter will be less exposed to ozone than actual surface molecules, as already discussed above. On the other hand, the lifetime of BaP molecules in the atmosphere can be shortened by additional loss processes like photolysis and reaction with other oxidants (OH, NO_2, NO_3, HNO_3, H_2SO_4, etc.).

Summary and Conclusions

In aerosol flow tube experiments at ambient temperature and pressure (296 K, 1 atm) the reaction of ozone with benzo[*a*]pyrene on spark discharge soot particles was found to proceed via a complex mechanism involving the reversible adsorption of O_3 and a subsequent surface reaction between adsorbed O_3 and BaP. The observed particle-related gas-phase ozone loss was independent of the BaP coating and occurred on a shorter time scale than the BaP decay. In the presence of water vapor both gas-phase ozone loss and BaP decay rates were reduced, which can be attributed to competitive adsorption of O_3 and H_2O. The investigated range of ozone volume mixing ratio and relative humidity was 0−1 ppm and 0−25%, respectively.

The adsorption processes can be described by Langmuir isotherms, and from nonlinear least-squares fits to four independent sets of BaP decay and ozone loss measurement data two independent and consistent estimates have been derived for the following parameters: Langmuir adsorption equilibrium constants for O_3 and H_2O, surface concentration of adsorption sites and maximum pseudo-first-order BaP decay rate coefficient. The preferred values are $K_{O_3} = (2.8 \pm 0.2) \times 10^{-13}$ cm^3, $K_{H_2O} = (2.1 \pm 0.4) \times 10^{-17}$ cm^3, $[SS]_S = (5.7 \pm 1.7) \times 10^{14}$ cm^{-2}, and $k_{1,\infty} = (0.015 \pm 0.001)$ s^{-1}.

On the basis of these results a second-order O_3−BaP surface reaction rate coefficient $k_{2,s} = (2.6 \pm 0.8) \times 10^{-17}$ cm^2 s^{-1} can be calculated. Taking into account literature values for the initial O_3 and H_2O sticking probabilities on soot surfaces also mean surface residence times for O_3 and H_2O were derived: $\tau_{O_3} \approx 5-18$ s and $\tau_{H_2O} \approx 3$ ms. Differing by almost 3 orders of magnitude, these residence times clearly suggest chemisorption of O_3 and physisorption of H_2O. They also allow the calculation of estimates for the adsorption enthalpies of ozone and water vapor: $\Delta H_{ads,O_3} \approx -(80-90)$ kJ mol^{-1}; $\Delta H_{ads,H_2O} \approx -50$ kJ mol^{-1}.

Since the gas-phase ozone loss and its reduction by H_2O were practically the same on BaP-coated and uncoated spark discharge soot particles, the adsorption equilibrium constants K_{O_3} and K_{H_2O} and the mean residence times τ_{O_3} and τ_{H_2O} can be expected to be similar on other graphene or PAH-like surface structures. Under dry conditions the half-life of surface BaP molecules was only ∼5 min in the presence of ozone at typical atmospheric volume mixing ratios around 30 ppb, and for 75% relative humidity it is estimated to increase to ∼45 min. Thus practically no BaP is expected to be present on the surface of aged atmospheric particles, since previous studies indicated similarly short half-lives of BaP on silica surfaces exposed to ozone, and since also other oxidants and photolysis will play a role in the atmosphere. In contrast, physical shielding effects are expected to prevent rapid oxidative degradation of BaP in the bulk of solid aerosol particles. For BaP contained in the bulk of liquid organic or aqueous surface layers or particles, on the other hand, physical shielding effects will be less pronounced and the rate of BaP degradation will depend in a complex way on the uptake and diffusion of oxidants from the gas phase as well as on the formation and consumption of reactive species by other chemical processes in the liquid. Thus, not only other PAH and gas-phase oxidants but also well-defined proxies for different particulate matrices should be investigated in future systematic studies of the degradation of particle-bound PAH in the atmosphere.

Acknowledgment. This work has been funded by the German Federal Ministry of Education and Research (BMBF Programs AFS and AFO2000). Experimental support by Susanna Mahler and stimulating discussions with Stefan Kamm and other members of the EUROTRAC scientific community are gratefully acknowledged.

References and Notes

(1) Finlayson-Pitts, B. J.; Pitts, J. N. *Chemistry of the Upper and Lower Atmosphere*, 1st ed.; Academic Press: San Diego, 2000.
(2) Heyder, J.; Gebhart, J.; Rudolph, F.; Schiller, C. F.; Stahlhofen, W. *J. Aerosol Sci.* **1986**, *17*, 814−825.
(3) Hannigan, M. P.; Cass, G. R.; Penman, B. W.; Crespi, C. L.; Lafleur, A. L.; Busby, W. F.; Thilly, W. G.; Simoneit, B. R. T. *Environ. Sci. Technol.* **1998**, *32*, 3502−3514.
(4) Cauwenberghe, K. V. Atmospheric Reactions of PAH. In *Handbook of Polycyclic Aromatic Hydrocarbons*; Bjorseth, A., Ramdahl, T., Eds.; Dekker: New York, 1985; pp 351−384.
(5) Kotzick, R.; Panne, U.; Niessner, R. *J. Aerosol. Sci.* **1997**, *28*, 725−735.
(6) Novakov, T.; Corrigan, C. E. *Geophys. Res. Lett.* **1996**, *23*, 2141−2144.
(7) Cruz, C. N.; Pandis, S. N. *Atmos. Environ.* **1997**, *31*, 2205−2214.
(8) Homann, K. H. *Angew. Chem.* **1998**, *37*, 2435−2451.
(9) Penner, J. E.; Chuang, C. C.; Grant, K. *Clim. Dyn.* **1998**, *14*, 839−851.
(10) Kirkevag, A.; Iversen, T.; Dahlback, A. *Atmos. Environ.* **1999**, *33*, 2621−2635.
(11) Ackerman, A. S.; Toon, O. B.; Stevens, D. E.; Heymsfield, A. J.; Ramanathan, V.; Welton, E. J. *Science* **2000**, *288*, 1042−1047.
(12) Kotzick, R.; Niessner, R. *Atmos. Environ.* **1999**, *33*, 2669−2677.
(13) Weingartner, E.; Baltensperger, U.; Burtscher, H. *Environ. Sci. Technol.* **1995**, *29*, 2982−2986.
(14) Disselkamp, R. S.; Carpenter, M. A.; Cowin, J. P.; Berkowitz, C. M.; Chapman, E. G.; Zaveri, R. A.; Laulainen, N. S. *J. Geophys. Res.* **2000**, *105*, 9767−9771.
(15) Kamm, S.; Möhler, O.; Naumann, K. H.; Saathoff, H.; Schurath, U. *Atmos. Environ.* **1999**, *33*, 4651−4661.
(16) Longfellow, C. A.; Ravishankara, A. R.; Hanson, D. R. *J. Geophys. Res.−Atmos.* **2000**, *105*, 24345−24350.
(17) Cooke, W. F.; Wilson, J. J. N. *J. Geophys. Res.* **1996**, *101*, 19395−19409.
(18) Reisinger, A. R. *Atmos. Environ.* **2000**, *34*, 3865−3874.
(19) Ammann, M.; Kalberer, M.; Jost, D. T.; Tobler, L.; Rossler, E.; Piguet, D.; Gaggeler, H. W.; Baltensperger, U. *Nature* **1998**, *395*, 157−160.
(20) Ammann, M.; Arens, F.; Gutzwiller, L.; Rössler, E.; Gäggeler, H. W. The Reaction of NO2 with Solid Anthracenetriol and Naphthalenediol. In *EC/Eurotrac-2 Joint Workshop Proceedings*; Ford Forschungszentrum: Aachen, 1999; pp 236−239.
(21) Warnatz, J.; Maas, U.; Dibble, R. W. *Combustion*; Springer: Berlin, 1999.
(22) Fendel, W.; Matter, D.; Burtscher, H.; Schmidt-Ott, A. *Atmos. Environ.* **1995**, *29*, 967−973.
(23) Helsper, C.; Mölter, W.; Löffler, F.; Wadenpohl, C.; Kaufmann, S.; Wenninger, G. *Atmos. Environ.* **1993**, *27A*, 1271−1275.
(24) Niessner, R. *Sci. Total Environ.* **1984**, *36*, 353−362.
(25) Eliasson, B.; Kogelschatz, U. *Ozone Sci. Eng.* **1991**, *13*, 365−373.
(26) Fitzer, E.; Fritz, W. *Technische Chemie: Einführung in die Chemische Reaktionstechnik*, 3rd ed.; Springer-Verlag: Berlin, 1989.
(27) VDI−Richlinie 2465, B. *Messen von Russ (Immission); Chemisch-analytische Bestimmung des elementaren Kohlenstoffes nach Extraktion und Thermodesorption des organischen Kohlenstoffes*; Beuth: Berlin, 1996.
(28) Willeke, K.; Baron, P. A. *Aerosol Measurement: Principles, Techniques, and Applications*; Van Nostrand Reinhold: New York, 1993.
(29) Reist, P. C. *Introduction to Aerosol Science*; Macmillan Publishing Company: New York, 1984.
(30) Karcher, W.; Fordham, R. J. *Spectral Atlas of Polycyclic Aromatic Compounds*; Kluwer Academic Publishers: Dordrecht, 1987; Vol 2.
(31) Murray, J. J.; Pottie, R. F.; Pupp, C. *Can. J. Chem.* **1974**, *52*, 557−563.
(32) Pöschl, U.; Canagaratna, M.; Jayne, J. T.; Molina, L. T.; Worsnop, D. R.; Kolb, C. E.; Molina, M. J. *J. Phys. Chem. A* **1998**, *102*, 10082−10089.
(33) Kolb, C. E.; Worsnop, D. R.; Zahniser, M. S.; Davidovits, P.; Keyser, L. F.; Leu, M.-T.; Molina, M. J.; Hanson, D. R.; Ravishankara, A. R.; Williams, L. R.; Tolbert, M. A. Laboratory Studies of Atmospheric

Heterogeneous Chemistry. In *Progress and Problems in Atmospheric Chemistry*; Barker, R., Ed.; World Scientific: Singapore, 1995; pp 771−875.

(34) Atkins, P. W. *Physical Chemistry*, 2nd ed.; Oxford University Press: London, 1982.

(35) Reid, R. C.; Prausnitz, J. M.; Poling, B. E. *The Properties of Gases and Liquids*, 4th ed.; McGraw-Hill Book Company: New York, 1987.

(36) Hanson, D. R. *J. Phys. Chem. B* **1997**, *101*, 4998−5001.

(37) Stephens, S.; Rossi, M. J.; Golden, D. M. *Int. J. Chem. Kinet.* **1986**, *18*, 1133−1149.

(38) Fendel, W.; Schmidt-Ott, A. *J. Aerosol Sci.* **1993**, *24*, S317−S318.

(39) Rogaski, C. A.; Golden, D. M.; Williams, L. R. *Geophys. Res. Lett.* **1997**, *24*, 381−384.

(40) Smith, D. M.; Chughtai, A. R. *J. Geophys. Res.* **1996**, *101*, 19607−19620.

(41) Ishiguro, T.; Takatori, T.; Akihama, K. *Combust. Flame* **1997**, *108*, 231−234.

(42) Chughtai, A. R.; Brooks, M. E.; Smith, D. M. *J. Geophys. Res.* **1996**, *101*, 19505−19514.

(43) Alcala-Jornod, C.; van den Bergh, H.; Rossi, M. J. *Phys. Chem. Chem. Phys.* **2000**, *2*, 5584−5593.

(44) Thomas, E.; Rudich, Y.; Trakhtenberg, S.; Ussyshkin, R. *J. Geophys. Res.* **1999**, *104*, 16053−16059.

(45) Rudich, Y.; Benjamin, I.; Naaman, R.; Thomas, E.; Trakhtenberg, S.; Ussyshkin, R. *J. Phys. Chem. A* **2000**, *104*, 5238−5245.

(46) Wu, C.-H.; Salmeen, I.; Niki, H. *Environ. Sci. Technol.* **1984**, *18*, 603−607.

(47) Cope, V. W.; Kalkwarf, D. R. *Environ. Sci. Technol.* **1987**, *21*, 643−648.

(48) Alebic-Juretic, A.; Cvitas, T.; Klasinc, L. *Environ. Sci. Technol.* **1990**, *24*, 62−66.

(49) Alebic-Juretic, A.; Cvitas, T.; Klasinc, L. *Chemosphere* **2000**, *41*, 667−670.

(50) Letzel, T.; Rosenberg, E.; Wissiack, R.; Grasserbauer, M.; Niessner, R. *J. Chrom. A* **1999**, *855*, 501−514.

(51) Koeber, R.; Bayona, J. M.; Niessner, R. *Environ. Sci. Technol.* **1999**, *33*, 1552−1558.

(52) Pitts Jr., J. N.; Paur, H.-R.; Zielinska, B.; Arey, J.; Winer, A. M.; Ramdahl, T.; Mejia, V. *Chemosphere* **1986**, *15*, 675−685.

(53) Kamens, R. M.; Guo, Z.; Fulcher, J. N.; Bell, D. A. *Environ. Sci. Technol.* **1988**, *22*, 103−108.

(54) McDow, S. R.; Vartiainen, M.; Sun, Q.; Hong, Y.; Yao, Y.; Kamens, R. M. *Atmos. Environ.* **1995**, *29*, 791−797.